Encoding strongly-correlated many-boson wavefunctions on a photonic quantum computer: application to the attractive Bose-Hubbard model

Saad Yalouz,[1, 2, *] Bruno Senjean,[3, 2, †] and Vedran Dunjko[4, ‡]

[1] *Theoretical Chemistry, Vrije Universiteit, De Boelelaan 1083, NL-1081 HV, Amsterdam, The Netherlands*

[2] *Instituut-Lorentz, Universiteit Leiden, P.O. Box 9506, 2300 RA Leiden, The Netherlands*

[3] *ICGM, Univ Montpellier, CNRS, ENSCM, Montpellier, France*

[4] *Universiteit Leiden, P.O. Box 9506, 2300 RA Leiden, The Netherlands*

Variational quantum algorithms (VQA) are considered as some of the most promising methods to determine the properties of complex strongly correlated quantum many-body systems, especially from the perspective of devices available in the near term. In this context, the development of efficient quantum circuit ansatze to encode a many-body wavefunction is one of the keys for the success of a VQA. Great efforts have been invested to study the potential of current quantum devices to encode the eigenstates of fermionic systems, but little is known about the encoding of bosonic systems. In this work, we investigate the encoding of the ground state of the (simple but rich) attractive Bose–Hubbard model using a Continuous-Variable (CV) photonic-based quantum circuit. We introduce two different ansatz architectures and demonstrate that the proposed continuous variable quantum circuits can efficiently encode (with a fidelity higher than 99%) the strongly correlated many-boson wavefunction with just a few layers, in all many-body regimes and for different number of bosons and initial states. Beyond the study of the suitability of the ansatz to approximate the ground states of many-boson systems, we also perform initial evaluations of the use of the ansatz in a variational quantum eigensolver algorithm to find it through energy minimization. To this end we also introduce a scheme to measure the Hamiltonian energy in an experimental system, and study the effect of sampling noise.

I. INTRODUCTION

In recent years, great efforts have been deployed to study the potential of noisy intermediate-scale quantum (NISQ) computers to tackle tasks that are hard to for classical computers. One of the most emblematic research lines in the field is the development of near-term algorithms to determine the properties of complex quantum many-body systems. Variational quantum circuits have shown to be very efficient and promising for encoding complex wavefunctions of various kinds of systems. Applications of these circuits range from molecular systems in quantum chemistry [1–11], interacting-spins and electrons models from condensed matter [12–14] or vibrational Hamiltonians [15], to cite but a few.

In practice, the efficiency of a variational quantum algorithm (VQA) depends on the expressibility of the quantum ansatz used to describe the wavefunction of the system under study. So far, this question has been extensively investigated in the case of qubit-based quantum circuits. Examples are the unitary coupled-cluster ansatz [16] introduced for electronic structure problems, adaptive methods designed to produce expressive ansatze at lower complexity cost [17, 18], and different strategies to solve condensed matter models with strong quantum correlation [12, 19]. The great majority of these works has been essentially devoted to the case of many-fermion systems. In contrast, little attention has been paid to the capability of current devices to produce interesting ansatze for the study of strongly interacting many-boson systems. While state-of-the-art methods such as quantum Monte-Carlo simulations have proved effective on classical computers [20–30], there is still a growing interest in conducting quantum experiments to treat many-boson systems, for instance based on superconducting circuits [31–34] or photonic quantum devices [35–41], essentially used as analog quantum simulators.

Motivated by the development of VQAs, we investigate the case of strongly correlated many-boson systems using a digital photonic-based Continuous Variable (CV) quantum computer [42–44]. In practice, CV devices are digital quantum computers that can manipulate information by entangling and measuring quantum states of light using various types of quantum gates. The bosonic nature of such photonic devices leads to a one-to-one mapping between the photonic modes of a CV computer and the bosonic modes of other many-boson systems. For variational algorithms, the CV setting is then particularly well-suited to explore new types of quantum circuit ansatz to encode strongly correlated many-boson wavefunctions. The rich complexity of such type of wavefunctions can be qualitatively reproduced by studying the attractive Bose–Hubbard (BH) model. The ground state of this model has attracted a lot of attention recently due to its rich transitional behavior that evolves between the so-called Schrödinger cat-like states to su-

---

* yalouzsaad@gmail.com
† bsenjean@gmail.com
‡ v.dunjko@liacs.leidenuniv.nl

perfluid regimes [45–51]. Furthermore, the BH model has been successfully employed to describe the physics of ultracold atoms and molecules in optical lattices [52–57], quantum cooling protocols [33] and the evolution of vibrational bosons in α-helices proteins [58, 59].

In this work, we propose two different CV quantum circuit ansatze dedicated to the encoding of many-boson wavefunctions. By performing VQAs based on the state-infidelity as a cost function, we show that the many-boson ground state of the BH model can be successfully realized on the CV quantum circuit with a relatively small number of gates and parameters. As the state-infidelity cannot be computed for large systems (as it requires the knowledge of the exact wavefunction), a realistic experiment on a true quantum devices requires the ability to measure the ground-state energy instead. Thus, we propose a photon-counting protocol to measure the expectation value of the BH Hamiltonian in order to simulate a variational quantum eigensolver (VQE) algorithm, as it would be done in a true experiment, with and without sampling noise.

The paper is organized as follows. After a brief introduction to the attractive BH Hamiltonian and the exact diagonalisation method in sections II A and II B, we illustrate the exotic structural transition of the BH ground state on three small-sized networks in section II C. After introducing the context of VQAs in section III A, we present the architectures of our proposed ansatze in section III B. Numerical investigations of their encoding ability are performed in section IV. We extend our study to ideal and realistic simulations of a VQE algorithm in section V. Finally, conclusions and perspectives are provided in section VI.

II. BOSE-HUBBARD MODEL

In this first section, we present a general introduction of the attractive BH model. Our objective is to give an overview of the properties of the model and to illustrate the rich behaviors that arise from the increase of the many-body interaction. We will focus on three small-sized BH models, namely the BH dimer and the three- and four-site periodic chains. These systems will be used later in this paper as test-bed for the quantum ansatze designed herein to encode many-boson wavefunctions on photonic devices.

A. Hamiltonian and regimes of interactions

The attractive BH model describes the physics of N_B bosons hopping between the N_S sites of a network with local attractive many-body interactions. The associated

Hamiltonian operator reads

$$\hat{\mathcal{H}} = -J \sum_{\langle p,q \rangle}^{N_S} (b_p^\dagger b_q + b_q^\dagger b_p) - \frac{U}{2} \sum_p^{N_S} n_p(n_p - 1), \quad (1)$$

where $J > 0$ is the hopping parameter describing the delocalization of the bosons throughout the connected nodes of the BH network, and $U > 0$ is the many-body interaction term corresponding to the local boson-boson interaction that occurs when at least two particles occupy the same site. In this work, J is the energy unit (*i.e.* we set $J \equiv 1$ in every simulation).

To characterize the competition between the many-body interactions and the hopping terms in the system, a dimensionless parameter

$$\Lambda = \frac{N_B U}{J} \quad (2)$$

is commonly introduced. Typically, $\Lambda \ll 1$ represents a regime of weak interaction (the so-called "Super-fluid regime") in which the physics of the system is governed by the hopping terms making the bosons able to efficiently delocalize over the network. The case $\Lambda \sim 1$ corresponds to an intermediate quantum regime where hoppings and local many-particle interactions compete together and where phase transitions usually occur. The last case, $\Lambda \gg 1$, corresponds to the regime where the many-body interaction dominates (the so-called "Fock regime"). In the case of attractive interactions, the resulting state tends to localize the bosons on local sites of the system (giving rise to macroscopic-cat states as illustrated later in this work).

B. Ground state reference: exact diagonalization

To investigate the exotic phases encoded in the attractive BH model, we compute the ground state of the Hamiltonian $\hat{\mathcal{H}}$ exactly by solving the time-independent Schrödinger equation

$$\hat{\mathcal{H}} |\Psi_0\rangle = E_0 |\Psi_0\rangle, \quad (3)$$

where $|\Psi_0\rangle$ is the ground state of the system with the associated energy E_0. We solve Eq. (3) by exact diagonalization (ED) (see Refs. 60 and 61 for an introduction of the technique) to obtain a good reference state to compare with our quantum ansatz developed for CV devices. The way ED works is simple: given a system of N_B bosons evolving on a network of N_S sites, one builds an exact matrix representation of the associated Hamiltonian and diagonalize it. In the case of the attractive BH model, the dimension $D_{\hat{\mathcal{H}}}$ of the resulting matrix is equal to the dimension of the Fock space of the system,

$$D_{\hat{\mathcal{H}}} = \frac{(N_B + N_S - 1)!}{N_B!(N_S - 1)!}, \quad (4)$$

N_S \ N_B	2	3	4	5	8	16
2	3	4	5	6	9	17
3	6	10	15	21	45	153
4	10	20	35	56	165	969
8	36	120	330	792	6435	245157

Table I. Evolution of the dimension $D_{\hat{\mathcal{H}}}$ of the BH model as a function of the number of sites N_S and bosons N_B.

which represents the number of ways of distributing N_B bosons on N_S sites. See Tab. I, for an overview of the scaling of the $D_{\hat{\mathcal{H}}}$ as a function of N_S and N_B.

While exact diagonalization provides access to the exact solution of the problem, the exponential scaling of the Fock space dimension with respect to the number of sites and bosons limits the use of ED to very small systems in practice.

C. Illustration of the different regimes of interaction: exact diagonalization on small systems

As the many-body interaction increases, the ground state of the attractive BH model exhibits rich transitional behaviors. Such transitions have already been extensively discussed in several recent works (see for example [48, 49, 51]). Here, we briefly illustrate some of these exotic phases in three systems (that will be treated later using quantum ansatze developed on a CV device), namely the BH dimer, the three-site and the four-site periodic chain.

We employ the Inverse Participation Ratio (IPR) [62–65] and the von Neumann entropy [66–68] as two indicators to follow the expansion of $|\Psi_0\rangle$ in the configuration basis when Λ increases. Applied to the Fock state basis, the IPR estimates the number of different bosonic configurations forming $|\Psi_0\rangle$ by linear combination, and reads

$$\text{IPR}(|\Psi_0\rangle) = \Big(\sum_{n_1,\ldots,n_{N_S}} |\langle n_1,\ldots,n_{N_S}|\Psi_0\rangle|^4 \Big)^{-1}, \quad (5)$$

where $|n_1,\ldots,n_{N_S}\rangle$ is a Fock state with n_q bosons on site q (and $\sum_q n_q = N_B$). Within this definition, a state $|\Psi_0\rangle$ localized on a single state of the Fock-state basis has an IPR of 1. By contrast, the IPR of a state uniformly delocalized over all the Fock states is equal to $D_{\hat{\mathcal{H}}}$.

The von Neumann entropy is a measure used to quantify the entanglement (non-local quantum correlation) existing between different sub-parts of a quantum system. In many-body systems, it quantifies the degree of entanglement and correlation arising between the subsystem p and all the other modes (also commonly called
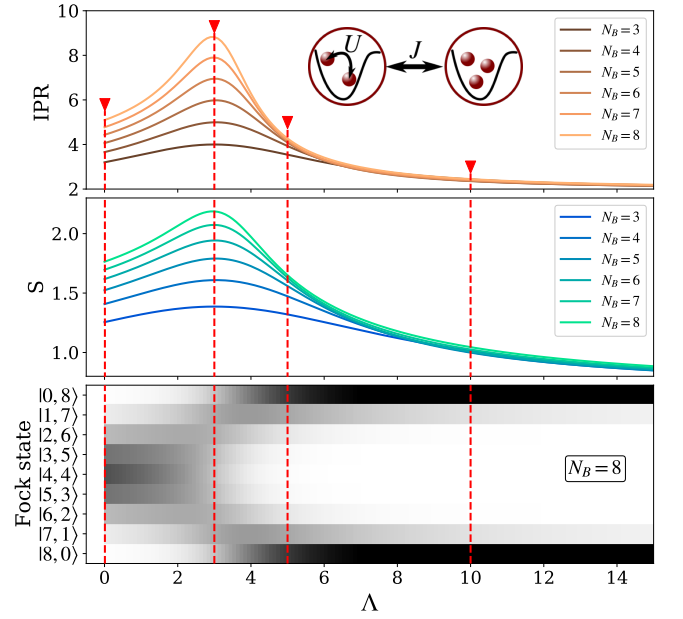

Figure 1. Evolution of the ground state structure of the dimer as a function of Λ (obtained with ED). **Upper panel:** IPR values for different values of total boson number $N_B = 2,\ldots,8$. **Middle panel:** Single site entropy value S values for different values of total boson number $N_B = 2,\ldots,8$. **Lower panel:** Occupancy probability of the ground state in the Fock state basis for $N_B = 8$. Probabilities are illustrated with shades of grey ranging from white for zero probability, to black for 50%.

"bi-partite entanglement"). It reads

$$S = -\sum_k \lambda_k \log(\lambda_k), \quad (6)$$

where λ_k are the eigenvalues of the reduced density matrix of mode p,

$$\hat{\sigma}_p = \sum_{n_k=0}^{N_B} \lambda_k |n_k\rangle \langle n_k|, \quad (7)$$

defined by taking the partial trace of the full-system density operator $\hat{\rho}$ over the Fock-state basis of all the other modes in the systems, $\hat{\sigma}_p = \text{Tr}_{q\neq p}[\hat{\rho}]$ (note that in our case, the full density operator is $\hat{\rho} = |\Psi_0\rangle \langle \Psi_0|$ as one focuses on the ground state). For the sake of simplicity, we will only focus on a single-site von-Neumann entropy as defined in Eq. (6).

In Figure 1, we show the evolution of the ground state properties of the BH dimer as a function of the interaction parameter Λ (for different fixed number of bosons N_B). When $\Lambda \sim 0$, the system is in a superfluid phase: every bosons propagate independently on the dimer and do no interact together. The independent-boson picture leads to a trivial product-state solution for the ground state as $|\Psi_0\rangle = \frac{1}{\sqrt{2}\sqrt{N_B!}}(a_0^\dagger + a_1^\dagger)^{N_B}|0,0\rangle$ (with $|0,0\rangle$ being the vacuum state of the dimer). Then, increasing Λ
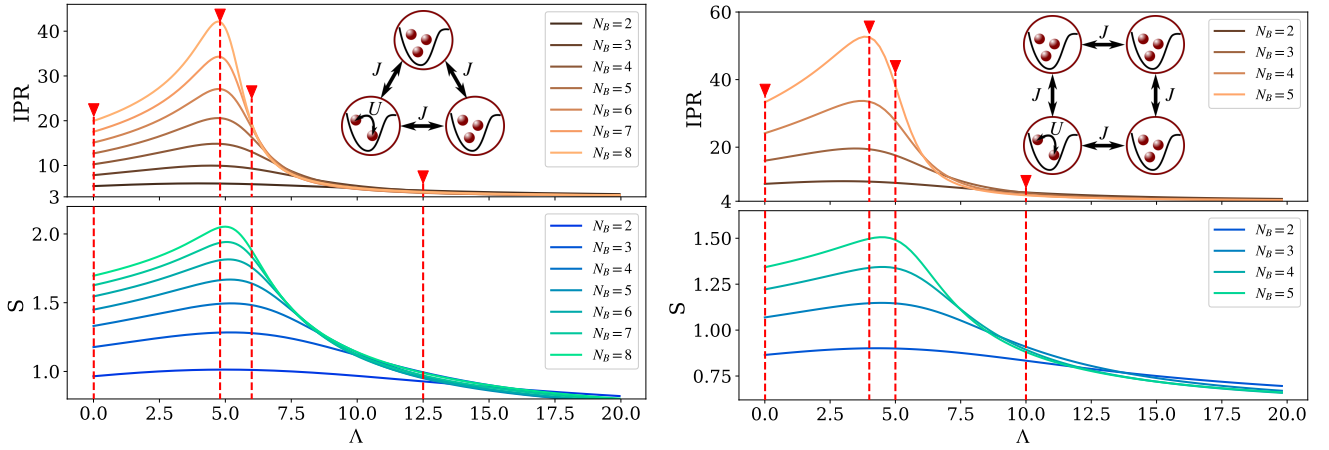
Figure 2. IPR and the single site von-Neumann entropy S of the attractive BH ground state as a function of N_B and Λ (obtained by ED). **Left panel:** Three-site BH periodic chain. **Right panel:** Four-site BH periodic chain. In both panels, the vertical dashed lines mark values of Λ representative of three different many-body regimes. These values will be used later on to illustrate the expressibility of our quantum ansatze on a CV circuit.

leads to a progressive restructuring of the ground state as readily seen by the increasing IPR. This shows a spreading of the state over the whole Fock basis that is also accompanied by an increasing single-site von-Neumann entropy. Both quantities then reach a maximum value for $\Lambda \approx 3$. The large variations of these two measures are not without significance and reveal the appearance of quantum correlations and entanglement in the system. Indeed, in the region $2 \leq \Lambda \leq 4$ the shape of the ground state gets more complex as it involves a larger number of bosonic configurations (actually almost all the Fock states are involved), and locally the bosonic modes get strongly entangled. Finally, as Λ increases the structure of the ground state loses in complexity and progressively tends to the well-known "cat-like" form [48, 49] representing a superposition of two macroscopically occupied states (*i.e.* $|\Psi_0\rangle = \frac{1}{\sqrt{2}}(|N_B, 0\rangle + |0, N_B\rangle)$). The IPR reaches a value of 2, thus indicating the importance of these two fully localized bosonic configurations. The entanglement entropy S of the modes decreases as less bosonic configurations get correlated. To better picture the full restructuring process occurring during this exotic quantum transition, we represent the decomposition of the BH dimer's ground state in the Fock basis as a function of Λ in the lower panel in Fig. 1.

Turning to larger systems, similar exotic quantum transitions can be observed. In Fig. 2 we see that the IPR and the single-site von-Neumann entropy also reach their maximal value around $\Lambda \approx 5$ for the three- and the four-site periodic chains. In this regime, the complexity of the ground state significantly grows with the total number of sites N_S but also with the total number of bosons N_B. As an illustration, there are around IPR$^{max} \approx 42$ bosonic configurations involved in the structure of the ground state at the maximum value of the IPR ($\Lambda \approx 4.8$) for the three-site BH model with $N_B = 8$.

This number gets even higher for the four-site model with $N_B = 5$ and $\Lambda \approx 4$ with a total number of IPR$^{max} \approx 55$ bosonic configurations. When Λ goes beyond this region of high complexity, we retrieve the so-called cat-states as indicated by the number of macroscopically-occupied states (IPR = 3 and 4 for the three and four-site systems, respectively, *e.g.* for the three-site model we have $|\Psi_0\rangle \propto |N_B, 0, 0\rangle + |0, N_B, 0\rangle + |0, 0, N_B\rangle$).

III. PHOTONIC-GATE-BASED ANSATZE

In the following, we introduce the different theoretical ingredients to encode the BH ground state on a photonic-gate-based device.

A. Variational Quantum Algorithms

VQAs represent state-of-the-art methods for NISQ devices that have been proficiently used to determine the ground state properties of various many-body systems (see for example [12, 16–19] and the recent review about VQAs [69]). The protocol of a VQA usually follows the steps: *i*) map the problem onto the quantum device, *ii*) use a quantum circuit as an "ansatz" to generate a trial state that encodes the wavefunction of the many-body system, *iii*) evaluate a given cost function by repeated measurements, *iv*) optimize the quantum gates parameters of the ansatz circuit to minimize the cost function governed by a variational principle. In practice, one applies a unitary transformation $U(\vec{\theta})$ with tunable gate parameters (formally represented by the vector $\vec{\theta}$) to trans-

form an initial state $|\Psi_{ini}\rangle$ into a trial state

$$|\Psi(\vec{\theta})\rangle = \hat{U}(\vec{\theta})|\Psi_{ini}\rangle. \qquad (8)$$

Often $|\Psi_{ini}\rangle$ is the "all-zero" state, but can be something else such as the Hartree–Fock state in electronic structure problems. If one seeks the ground state of a system, the cost function is usually the ground-state energy defined as

$$E(\vec{\theta}) = \langle\Psi(\vec{\theta})|\hat{\mathcal{H}}|\Psi(\vec{\theta})\rangle \geq E_0, \qquad (9)$$

where E_0 is the exact ground-state energy and is a lower bound to the ground-state energy of the trial state $|\Psi(\vec{\theta})\rangle$. In a real VQA experiment, the expectation value $E(\vec{\theta})$ is estimated by statistical sampling. The energy estimator will have an uncertainty based on the number of state preparations and measurements used. This energy is then passed to an external classical optimization routine which provides a new set of parameters $\vec{\theta}$ used to update the quantum circuit. The whole optimization process is repeated until global convergence is reached (i.e. until $E(\vec{\theta})$ is minimized).

The efficiency of the VQA lies in the capability of the unitary $\hat{U}(\vec{\theta})$ to encode the ground state of the system, *i.e.* it has to show a strong "expressibility" so that the transformation given in Eq. (8) can efficiently map the initial state $|\Psi_{ini}\rangle$ to the exact ground state $|\Psi_0\rangle$. The question of the expressibility of quantum ansatze is hard to tackle and remains an open question in the quantum computing community. Only a few works have tried to investigate this problem on qubit devices with a special emphasis on many-electron problems (see for example the study of the unitary couple-cluster-ansatz in [70]), and one relies more on numerical evidence. A lot of attention has been directed to many-fermion systems (see for example [12, 17–19, 71–73]), but little work has been done on quantum ansatze to encode many-boson wavefunctions (for a notable exception, see the implementation of the unitary vibrational-coupled-cluster ansatz introduced in Ref. 15).

B. Photonic quantum circuits as ansatze for many-boson wavefunction

In contrast to most of the studies focusing on qubit devices, we tackle the problem using CV circuits. The choice of using CV devices to describe many-boson problems is rather intuitive as there exists a straightforward one-to-one correspondence between the modes of a bosonic system and the photonic modes of the CV device. In the case of the attractive BH system, each photonic mode p of the quantum circuit can be used to encode the bosonic population of the associated site p, as illustrated in Fig. 3. Starting from this advantageous property, we will build VQAs based on CV quantum circuits to en-
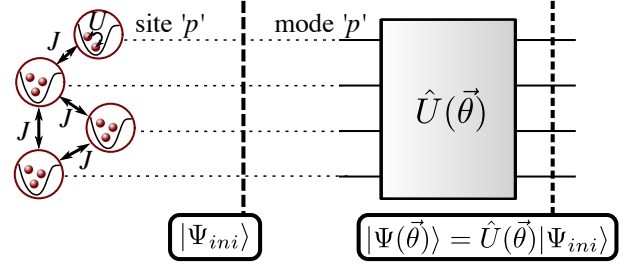

Figure 3. Illustration of a VQA approach where each photonic mode in the quantum circuit encodes the bosonic occupation of a particular site in the Bose-Hubbard network.

code a many-boson wavefunction trial state as defined in Eq. (8).

1. Utilized CV quantum gates

Concerning the basic properties of the ansatz, we know that the BH Hamiltonian in Eq. (1) is boson-number-preserving by construction (*i.e.* N_B is a constant of the problem). Thus, we restrict ourselves to three types of photon-number-preserving gates, namely beam-splitters, rotation gates and Kerr gates. The beam-splitter gate is a two-mode gate that affects two inputs modes simultaneously (labeled here p and q) and whose unitary is defined as

$$B_{p,q}(\theta,\phi) = \exp\left(\theta(e^{i\phi}a_q^\dagger a_p - e^{-i\phi}a_p^\dagger a_q)\right), \qquad (10)$$

where θ and ϕ are respectively the transmittivity and phase angle of the gate. The action of the beam-splitter's unitary on the associated ladder operators ($a_p/a_p^\dagger$ and $a_q/a_q^\dagger$) is given by

$$B_{p,q}(\theta,\phi)^\dagger a_p B_{p,q}(\theta,\phi) = a_p\cos(\theta) - a_q\sin(\theta)e^{-i\phi},$$
$$B_{p,q}(\theta,\phi)^\dagger a_q B_{p,q}(\theta,\phi) = a_q\cos(\theta) + a_p\sin(\theta)e^{i\phi}. \qquad (11)$$

To have a better illustration of the effects of the beam-splitter gate on a many-photon wavefunction, figure 4 shows the evolution of the density of probability of a two mode-state $B(\theta,0)|\Psi_{ini}\rangle$ (with $|\Psi_{ini}\rangle = |8,0\rangle$ or $|4,4\rangle$) in the Fock basis as a function of the transmittivity parameter θ. As shown in this figure, the main effect of the beam-splitter is to delocalize the photons from a mode to another one creating various patterns in the Fock basis. The latter strongly depend on the initial state considered.

Turning to the rotation gate, it affects the associated Fock state as $R_p(\theta)|n_p\rangle = e^{i\theta n_p}|n_p\rangle$ with the unitary operator defined as

$$R_p(\theta) = \exp\left(i\theta a_p^\dagger a_p\right). \qquad (12)$$

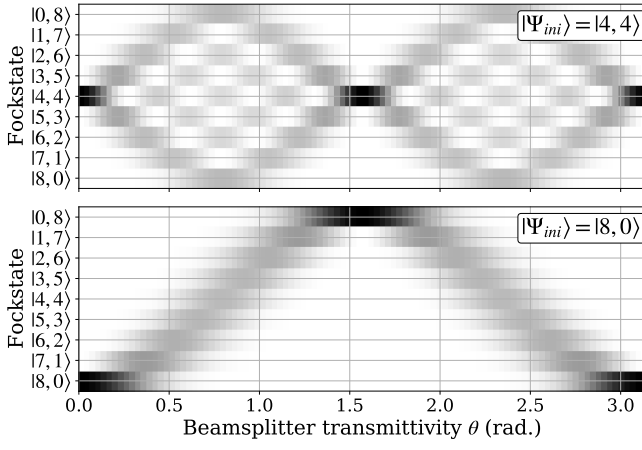Finally, the Kerr gate is a non-Gaussian single-mode gate

Figure 4. Density of probability of a state $B(\theta, 0)\left|\Psi_{ini}\right\rangle$ in the Fock basis as a function of the transmittivity parameter θ of the beam-splitter unitary. The probability is illustrated with shades of grey ranging from white for zero to black for unity. **Upper panel:** $\left|\Psi_{ini}\right\rangle = \left|4, 4\right\rangle$. **Lower panel:** $\left|\Psi_{ini}\right\rangle = \left|8, 0\right\rangle$
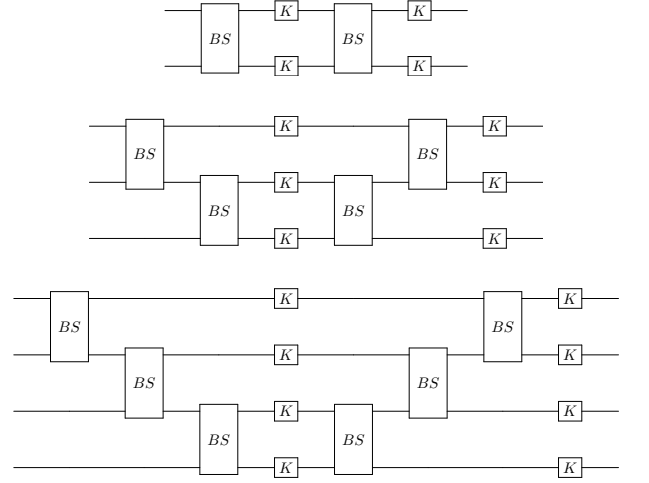
Figure 5. Structure of the BS-Kerr ansatz for $N_S = 2$, 3 and 4 sites with two consecutive layers. Each layer is composed of a series of $N_S - 1$ beam-splitter gates in stairs (up or down) followed by a series of N_S Kerr gates applied on each modes. The total gate count is $N_L(2N_S - 1)$ where N_L is the number of layers.

whose unitary reads

$$K_p(\theta) = \exp\left(i\theta(a_p^\dagger a_p)^2\right). \tag{13}$$

For a given modes p, this leads to $K_p(\theta)\left|n_p\right\rangle = e^{i\theta n_p^2}\left|n_p\right\rangle$, thus generating a non-linear phase term that depends on the squared number of bosons present in the mode p, $n_p^2 = (a_p^\dagger a_p)^2$. In the current devices, Kerr gates represent expensive resources which can only be implemented non-deterministically. Nonetheless, our analysis shows that they play a key role in the performance of our ansatze.

2. Minimal beam-splitter-Kerr ansatz

Let us now introduce our first ansatz to encode the ground state of the attractive BH model, that we call the minimal beam-splitter-Kerr (BS-Kerr) ansatz. This ansatz was designed to efficiently work with as few quantum gates and parameters to optimize as possible, based on numerical investigations. The most efficient architecture we found (in terms of the total number of gates required to encode the ground state with sufficient accuracy) resulted in layers of beam-splitter and Kerr gates as shown in Fig. 5 for two consecutive layers. Note that the phase angle parameters of the beam-splitters are always set to $\phi = 0$ in this ansatz. Indeed, we did not see any improvement when considering the latter in our numerical simulations (not shown). Discarding allows to reduce the complexity of the classical optimization with no impact on the final accuracy.

As readily seen in Fig. 5, each layer is defined as a series of $N_S - 1$ beam-splitter gates in stairs (up or down) followed by a series of N_S Kerr gates applied on each

mode, thus leading to a gate count of $N_L(2N_S - 1)$ (and the same number of parameters to optimize) where N_L is the number of layers. From a layer to another one, we alternate the stair structure to ensure that each mode can have the opportunity to exchange photons (via the beam-splitters) with all the other ones in the circuit.

Note that removing the Kerr gates from the ansatz led to very poor results (not shown), thus demonstrating the significant role of non-linearity to encode the ground state of the attractive BH model. Although there are materials that exhibit the $\chi^{(3)}$ non-linearity that is required for the Kerr interaction, the experimental realization of a Kerr gate remains a challenge at the present moment [74]. Despite such technological obstacle, there is still place for improvements on the implement of non-linear quantum gates [75].

3. Interferometer-Kerr ansatz

The BS-Kerr ansatz was designed to encode the ground state of the attractive BH model with a minimal number of gates and parameters, which is optimal in numerical simulation. However, in the experimental realization one wants to have an optimal use of the investigation tools (such as interferometers) and, if possible, to reduce the number of Kerr gates that are difficult to implement. Therefore, we considered an (more experimentally-friendly) alternative ansatz composed of layers of one interferometer and one Kerr gate per mode, as depicted in Fig. 6 for 3 and 4 modes. The interferometer is composed of $N_S(N_S - 1)/2$ beam-splitters and N_S rotation gates, making a total of $N_L N_S(N_S + 3)/2$ gates
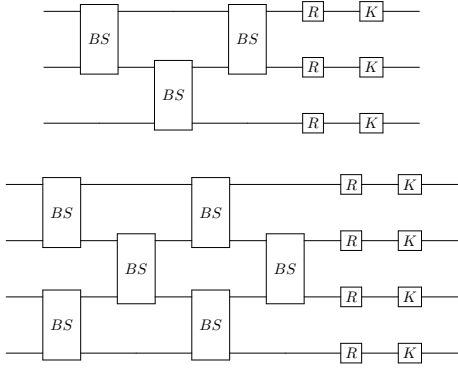
Figure 6. Single layer of the Interferometer-Kerr ansatz for $N_S = 3$ (top) and $N_S = 4$ (bottom) modes.

Figure 7. **BH dimer**. Minimum depth required (in terms of number of layer N_L and gate count) to generate a fidelity $\mathcal{F} \geq 99\%$ [see Eq. (14)] for different values of Λ and N_B. **Upper panel:** results obtained with the monomodal initial state. **Lower panel:** results obtained with the bimodal intial state.

and $N_L N_S (N_S + 1)$ parameters (as one beam-splitter accounts for two parameters).

At first sight, this ansatz appears less efficient than the BS-Kerr ansatz in terms of number of gates and parameters per layer. However, we can expect the additional expressivity brought about by the interferometers to lead to a reduction in the number of layers required to encode the ground state. In other words, the interferometer-Kerr ansatz could lead to a reduction in the total number of Kerr gates at the expense of additional beam-splitter and rotation gates. This hypothesis is numerically investigated in Sec. IV B.

The complexity of the ansatz can be reduced by getting rid of the rotation gates (physically irrelevant for most applications [76]) and/or setting the phase angles of all beam-splitters to $\phi = 0$ (and keeping only the transmittivity angles) as already done for the BS-Kerr ansatz.

IV. NUMERICAL INVESTIGATION OF THE ANSATZE EXPRESSIBILITY

In this section, we present our numerical results focusing on the encoding capacity of the two ansatze introduced previously applied to the BH dimer, the three-site and the four-site periodic chains. The simulations of the photonic circuits were realized using the Python package Strawberryfields [77]. For the optimization of the quantum circuits parameters, the L-BFGS-B method was used and encoded in the OptimParrallel package [78]. The circuit's parameters were always initialized with an amplitude randomly drawn in $[-0.05, +0.05]$, and the maximum number of iterations was set to 20000. A homemade ED code has been implemented in Python to compute the exact ground state by exact diagonalization.
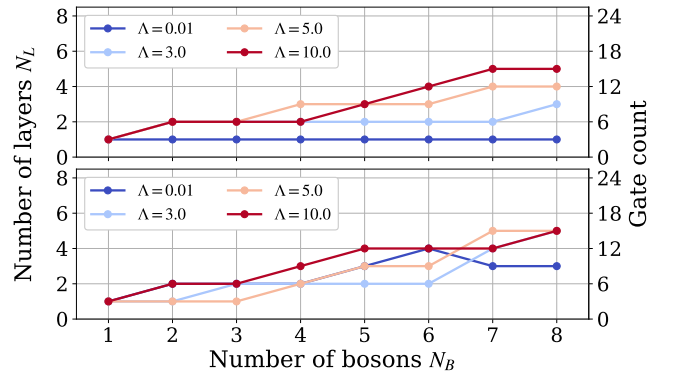
A. Capacity of the BS-Kerr ansatz

To demonstrate the capacity of the different ansatze to encode the ground state of BH networks, we estimated the fidelity of the trial state with respect to the exact ground state of the system $|\Psi_0\rangle$,

$$\mathcal{F} = |\langle \Psi_0 | \hat{U}(\vec{\theta}) | \Psi_{ini} \rangle|^2. \tag{14}$$

Assuming that the classical optimization process does not end up in local minima, an ansatz with a strong encoding capability will return a fidelity $\mathcal{F}$ close to unity. We numerically check this property by optimizing the quantum circuit's parameters to minimize a complementary measure that is the infidelity

$$\mathcal{I} = 1 - \mathcal{F} \tag{15}$$

that is naturally lower-bounded by zero. In the spirit of Ref. 12 on the Fermi–Hubbard model, we progressively increase the number of layers in the quantum circuits and perform a VQA where the infidelity is used as a cost function. As the number of layers increases, so does the expressibility of the ansatz in practice. We continue to increase the number of layers until the fidelity of the ground state reaches at least $\mathcal{F} \geq 99\%$ (conversely $\mathcal{I} < 1\%$). Note that no mention has been made so far about the nature of the initial state $|\Psi_{ini}\rangle$, for which we considered two choices: a monomodal and a bimodal states, detailed later in section IV A 1.

1. BH model with $N_S = 2$ sites

Focusing first on the BS-Kerr ansatz for the BH dimer, the minimum number of layers required to reach $\mathcal{F} \geq$
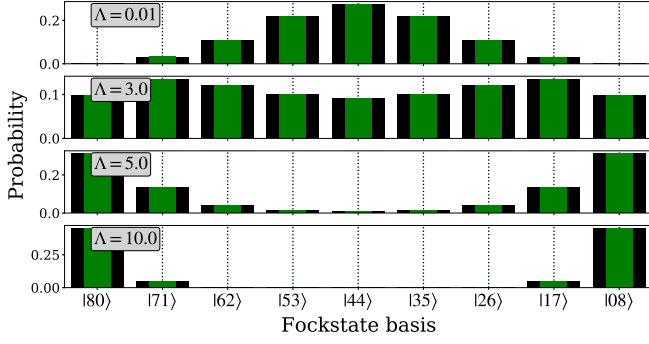
Figure 8. **BH dimer**. Probability of occupation of the ground state in the Fock basis obtained by the BS-Kerr ansatz (green bars) with $N_L = 6$, $N_B = 8$, $|\Psi_{ini}\rangle = |4, 4\rangle$ and different values of Λ. Results are compared with exact diagonalization (black bars).

99% for $N_B = 1$ to $N_B = 8$ is shown in Fig. 7 for Λ values corresponding to different regimes of correlation (as marked by the vertical red-dashed lines in Fig. 1). Two different initial states were considered: a monomodal one given by $|\Psi_{ini}\rangle = |N_B, 0\rangle$ and a bimodal one given by $|\Psi_{ini}\rangle = |\frac{N_B}{2}, \frac{N_B}{2}\rangle$ (*n.b.* for odd total number of bosons we took $|\Psi_{ini}\rangle = |\frac{N_B+1}{2}, \frac{N_B+1}{2} - 1\rangle$ instead). As a first general remark, a fidelity higher than 99% is reached in all cases (whatever the values of correlation strength Λ, the number of bosons N_B and the choice of initial state). This clearly demonstrates the potential of CV devices to efficiently encode the many-boson ground state of the attractive BH dimer even in the strongly correlated regime. Note that to generate an efficient encoding of the wavefunction, the larger N_B is the larger the number of layers N_L needs to be. This is expected as the complexity of the ground state grows with the size of the Fock space $D_{\hat{\mathcal{H}}}$, which is linear in N_B for the BH dimer as shown in Tab. I). Interestingly, the trend of the curves ensuring an efficient encoding is globally sub-linear in N_B. In other words, choosing a number of layers such as $N_L \approx 0.7 \times N_B$ seems to guarantee a very high ground-state fidelity in all cases considered herein. Another interesting fact is that in the weakly correlated case, $\Lambda = 0.01$, a single layer of the BS-Kerr ansatz is sufficient to reach a fidelity higher than 99%, even when the number of bosons increases. This is true only when the monomodal mode is used as the initial state. We rationalize this result in Appendix A, where we show that starting from the monomodal state, an exact encoding ($\mathcal{F} = 100\%$) of the BH ground state can be realized using only beamsplitters.

Furthermore, we computed the probability of occupation of our trial ground state in the Fock basis, shown in Fig. 8. This illustrates the structural transition of the BH dimer's ground state as a function of Λ for $N_B = 8$ bosons and $N_L = 6$ layers. In this case, we clearly see the structural transformation of the dimer ground state as Λ increases, starting from the superfluid regime
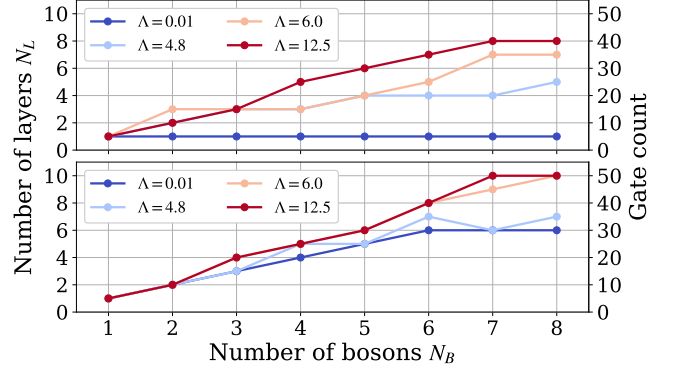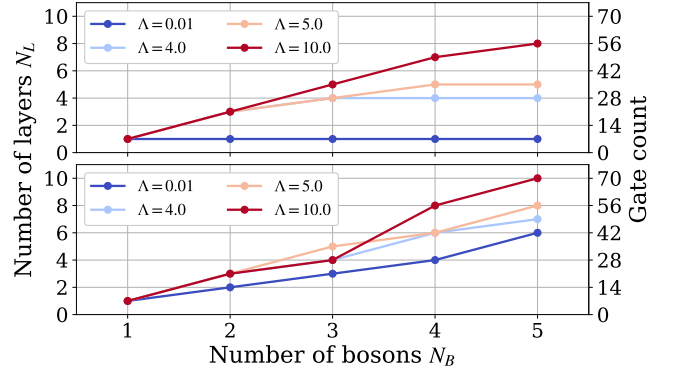

Figure 9. **3-site BH model**. Minimum depth required (in terms of number of layer N_L and gate count) to generate a fidelity $\mathcal{F} \geq 99\%$ [see Eq. (14)] for different values of Λ and N_B. **Upper panel:** results obtained with a monomodal initial state. **Lower panel:** results obtained with a bimodal intitial state.

Figure 10. **4-site BH model**. Minimum depth required (in terms of number of layer N_L and gate count) to generate a fidelity $\mathcal{F} \geq 99\%$ [see Eq. (14)] for different values of Λ and N_B. **Upper panel:** results obtained with the monomodal initial state. **Lower panel:** results obtained with the bimodal intitial state.

($\Lambda = 0.01$) and going through the maximum spreading structure ($\Lambda = 3$) to finally reach the famous "cat-like" superposition ($\Lambda = 5$ to 10). For all values of Λ, the probability of occupation of our trial state (green bars) is on top of the exact one (black bars) thus showing how efficient our quantum ansatz is to encode every exotic structures adopted by the ground state through its transitions.

2. *BH model with $N_S = 3$ and 4 sites*

Turning to larger systems, Figs. 9 and 11 show the results obtained on the three-site BH model for Λ values corresponding to different regimes of correlation (as marked by the vertical red-dashed lines in the left

panel Fig. 2). A monomodal and bimodal initial states are again considered and read $|\Psi_{ini}\rangle = |N_B, 0, 0\rangle$ and $|\Psi_{ini}\rangle = |\frac{N_B}{2}, 0, \frac{N_B}{2}\rangle$ respectively (*n.b.* for odd total number of bosons we took $|\Psi_{ini}\rangle = |\frac{N_B+1}{2}, 0, \frac{N_B+1}{2} - 1\rangle$ instead). Compared to the BH dimer, the dimension of the Fock space is non-linear in N_B (see Tab. I) thus leading to a maximum number of bosonic configurations accessible of $D_{\hat{\mathcal{H}}} = 45$ when $N_B = 8$ (approximately 6 times larger than the number of configurations on the dimer for the same number of bosons). In spite of this, we observed that the BS-Kerr ansatz performs very well as shown in Fig. 9. In this case, we retrieve some differences between the results obtained with the two initial states. The monomodal initial state seems to perform better and less layers are globally required to encode the ground state with a fidelity higher than 99%. As for the BH dimer, only one layer is required for $\Lambda = 0.01$ when this initial state is used.

Still, the ansatz is clearly able to efficiently transform both initial states into a very good approximation to the exact ground state. As readily seen in Fig. 9, choosing a circuit depth with $N_L \sim 1.25 \times N_B$ guaranties an efficient encoding of the ground state in all cases considered here for the attractive three-site BH model.

The complexity grows even stronger for the four-site BH network. We follow the exact same strategy than for the previous models by considering $|\Psi_{ini}\rangle = |N_B, 0, 0, 0\rangle$ as the monomodal initial state and $|\Psi_{ini}\rangle = |\frac{N_B}{2}, 0, \frac{N_B}{2}, 0\rangle$ as the bimodal one (*n.b.* for odd total number of bosons we took $|\frac{N_B+1}{2}, 0, \frac{N_B+1}{2} - 1, 0\rangle$ instead), as well as Λ values corresponding to different regimes of correlation marked by the vertical red-dashed lines in the right panel Fig. 2. For this system, the dimension of the Fock space explodes very quickly and fixing $N_B = 5$ already leads to a number of bosonic configurations of $D_{\hat{\mathcal{H}}} = 56$ that is larger than the size of the Fock space of the three-site model with $N_B = 8$. In our simulations, we chose to limit ourselves to a maximal number of bosons of $N_B = 5$ due to the numerical complexity of the classical simulation of our VQA. The performance of the BS-Kerr ansatz for $N_B = 1$ to 5 is shown in Fig. 10. In the full range of correlation regimes, the photonic circuit is again able to encode the ground state with high fidelity for a circuit depth of $N_L \approx 2N_B$.

As a complement, Figs. 11 and 12 illustrate the structural transition of the BH ground state for the three and four-site BH networks, respectively. Just as in the BH dimer, the density of probability of our trial ground state matches perfectly the one of the exact ground state. A remarkable property is that we always consider a single bosonic configuration as an initial state $|\Psi_{ini}\rangle$. Starting from this, the quantum circuit can efficiently transform the latter into a very complex linear combination of $D_{\hat{\mathcal{H}}}$ configurations encoding strong quantum correlations.
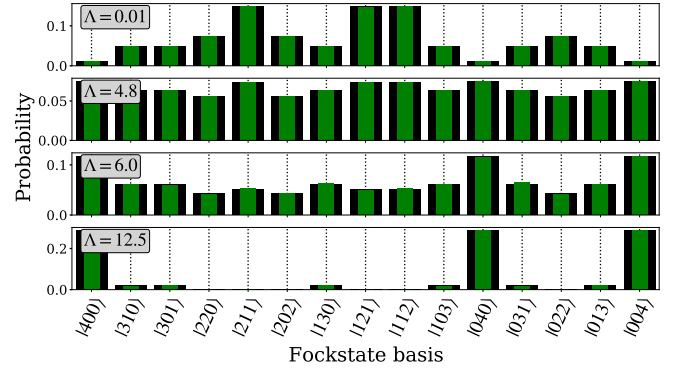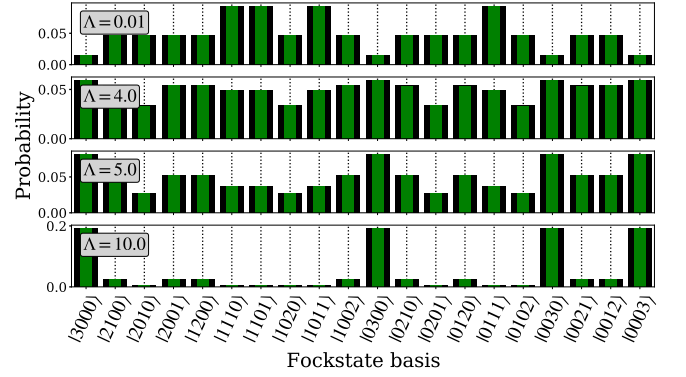

Figure 11. **3-site BH model**. Probability of occupation of the ground state in the Fock basis obtained by the BS-Kerr ansatz (green bars) with $N_L = 6$, $N_B = 4$, $|\Psi_{ini}\rangle = |2, 0, 2\rangle$ and different values of Λ. Results are compared with exact diagonalization (black bars).

Figure 12. **4-site BH model** Probability of occupation of the ground state in the Fock basis obtained by the BS-Kerr ansatz (green bars) with $N_L = 6$, $N_B = 3$, $|\Psi_{ini}\rangle = |2, 0, 1, 0\rangle$ and different values of Λ. Results are compared with exact diagonalization (black bars).

B. Capacity of the interferometer-Kerr ansatz

Let us now turn to the interferometer-Kerr ansatz described in Sec. III B 3. By using an interferometer composed of more beam-splitter and rotation gates, the interferometer-Kerr ansatz is expected to perform as efficiently as the BS-Kerr ansatz but with a reduced number of layers, hence a reduced number of Kerr gates. As readily seen in the top panel of Fig. 13, only $N_L = 6$ layers are necessary to encode more than 99% of the ground state of the three-site model for $N_B = 8$, compared to the 10 layers required by the BS-Kerr ansatz. Note that reducing the number of layers in the interferometer-Kerr ansatz does not necessarily reduce the total number of gates compared to the BS-Kerr ansatz. Indeed, $N_L = 6$ layers in the interferometer-Kerr ansatz is equivalent to 54 gates, while $N_L = 10$ for the BS-Kerr ansatz gives 50 gates. However, the number of Kerr gates is always directly proportional to the number of layers and the num-
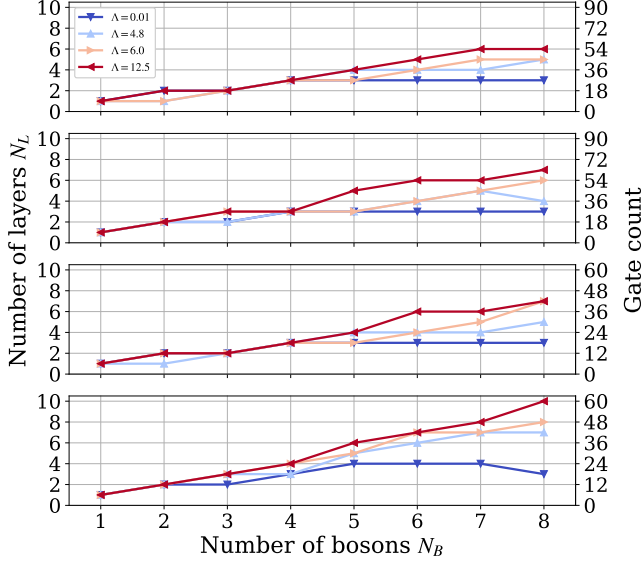
Figure 13. **3-site BH model**. Minimum depth required (in terms of number of layer N_L and gate count) to generate a fidelity $\mathcal{F} \geq 99\%$ [see Eq. (14)] for different values of Λ and N_B, using the bimodal initial state. **First panel:** Full ansatz, **Second panel:** Phase angles of the beam-splitters are set to 0, **Third panel:** Phase angles of the beam-splitter are reintroduced but rotation gates are removed, **Fourth panel:** Phase angles of the beam-splitters are set to 0 and the rotation gates are removed.

Figure 14. **4-site BH model**. Minimum depth required (in terms of number of layer N_L and gate count) to generate a fidelity $\mathcal{F} \geq 99\%$ [see Eq. (14)] for different values of Λ and N_B, using the bimodal initial state. **First panel:** Full ansatz, **Second panel:** Phase angles of the beam-splitters are set to 0, **Third panel:** Phase angles of the beam-splitter are reintroduced but rotation gates are removed, **Fourth panel:** Phase angles of the beam-splitters are set to 0 and the rotation gates are removed.

ber of modes as $N_{\mathrm{Kerr}} = N_L \times N_S$ such that the number of Kerr gates is almost reduced by half when using the interferometer-Kerr ansatz (designed for this exact purpose). Note that the phase angles of the beam-splitter gates were not set to 0 compared to the BS-Kerr ansatz. For a more fair comparison, we set them to 0 in the second panel of Fig. 13. One can notice a slight increase in the number of layers, especially when the correlation strength Λ increases, but only up to $N_L = 7$. Hence, for the three-site model, the interferometer-Kerr ansatz guaranties an efficient encoding of the ground state with $N_L \sim 0.8 N_B$ compared to $N_L \sim 1.25 N_B$ for the BS-Kerr ansatz, for all values of Λ.

We just saw that the total number of gates of the interferometer-Kerr ansatz can still be higher than of the BS-Kerr ansatz, despite a significant reduction in the number of Kerr gates. As mentioned in Ref. 76, the rotation gates of the interferometer are physically irrelevant for most applications. These gates are removed from the ansatz in the third and fourth panels of Fig. 13, where the phase angles of the beam-splitter are either free or set to 0, respectively. Looking at the fourth panel, it is clear that simultaneously removing the phase angles of the beam-splitter gates and the rotation gates deteriorates the performance of the ansatz, and does not lead to any improvement over the BS-Kerr ansatz. Even for $\Lambda = 0.01$, this is the only case where more than $N_L = 3$ layers are required to accurately encode the ground state.
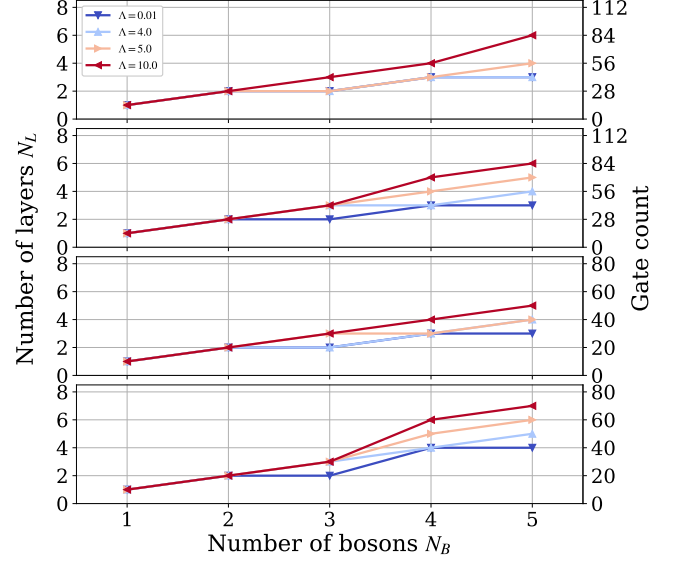
However, removing the rotation gates while keeping the phase angle of the Beam-Slitter gates (third panel) seems equivalent to doing the exact opposite, i.e. keeping the rotation gates and removing the phase angle of the beam-splitter gates (second panel). By doing so, the number of parameters remains the same but the total number of gates can be reduced, for instance from 63 to 42 for $N_B = 8$.

Turning to the four-site model in Fig. 14, we reach the exact same general conclusions as for the three-site model. It seems that the circuit depth required to encode the ground state of this model tends to $N_L \sim 1.2 N_B$, which again improves over $N_L \sim 2 N_B$ for the BS-Kerr ansatz. Without the rotations and the phase angles (fourth panel), the number of layers tends to increase in all regimes of correlation, while keeping the phase angles and removing the rotation gates seems to provide the best trade-off between the total number of gates, the number of Kerr gates (proportional to the number of layers), and the number of parameters.

V. VQE SIMULATIONS USING THE BS-KERR ANSATZ

In the previous section, we gave numerical evidence on the capacity of our proposed ansatze to encode the
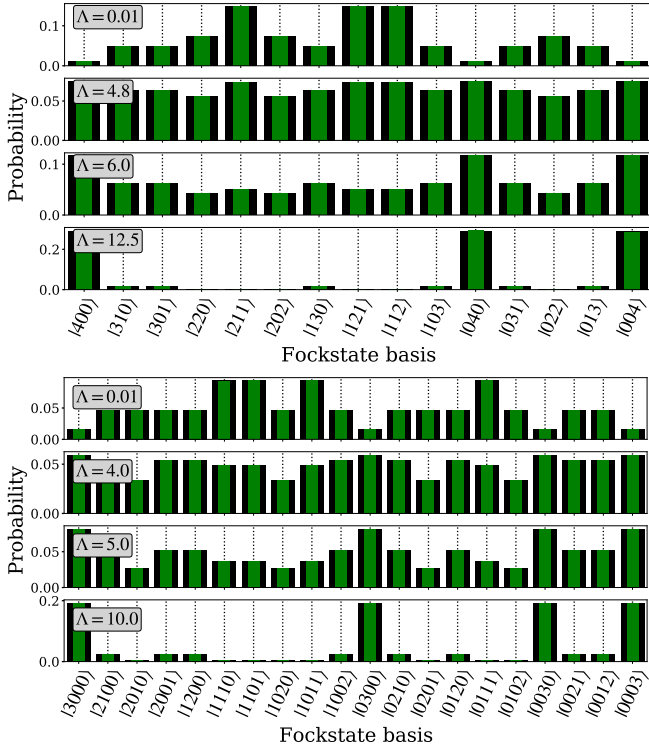
Figure 15. Probability of occupation in the Fock basis, obtained by ED (black bars) and VQE simulations with the BS-Kerr ansatz (green bars). All parameters were initialized with random amplitudes drawn in $[-0.05, +0.05]$, and the BFGS optimizer with a maximum number of 2000 iterations were used. **Upper panel:** Ground state of the three-site model with $N_B = 4$, $N_L = 6$ and $|\Psi_{ini}\rangle = |2,0,2\rangle$ **Lower panel:** Ground state of the four-site model with $N_B = 3$, $N_L = 6$ and $|\Psi_{ini}\rangle = |2,0,1,0\rangle$.

ground state of the attractive BH model. In this section, we switch to more practical calculations by simulating VQE protocols where the cost function to minimize is the energy of the system,

$$E(\vec{\theta}) = \langle \Psi_{ini} | U(\vec{\theta})^\dagger H U(\vec{\theta}) | \Psi_{ini} \rangle \geq E_0. \qquad (16)$$

For the sake of conciseness, we focus on the BS-Kerr ansatz only. First, we briefly demonstrate the accuracy of the results obtained on the three and four-site BH models. Second, we use the BH dimer as a test-bed to tackle the practical simulation of a VQE experiment on a CV device. This second part will be the occasion to compare the results obtained with an ideal realization of a VQE to a more realistic one, where the estimation of the energy $E(\vec{\theta})$ is based on a photon-counting protocol.

A. Ideal VQE simulations for the three- and four-site BH model

In this section, ideal simulations of the VQE algorithm are realized (*i.e.* infinite sampling, no photon loss, no error in the circuit. . .). This means that we assume that we can extract the trial state $|\Psi(\vec{\theta}) = U(\vec{\theta}) |\Psi_{ini}\rangle$ at the end of the circuit, which makes it possible to exactly estimate the energy $E(\vec{\theta})$ during the optimization process.

Figure 15 shows the probability of occupation in the Fock basis of the ground states obtained at the end of the VQE algorithm for different Λ values (consistent with the simulations realized in the previous section). Note that $N_L = 6$ layers and initial bimodal states ($|\Psi_{ini}\rangle = |2,0,2\rangle$ and $|\Psi_{ini}\rangle = |2,0,1,0\rangle$) are considered. The depth of the circuits imposes to optimize 30 (respectively 40) parameters for the three-site (four-site) network.

As shown in Fig. 15, the probability of occupation follows the same trend as the previous ones in Figs. 11 and 12, where the infidelity $\mathcal{I}$ was minimized instead of the ground-state energy. In all cases of Fig. 15, the resulting states have fidelity $\mathcal{F} \geq 99\%$ and an energy error $\Delta E = E(\vec{\theta}^*) - E_0 \leq 10^{-5} J$ (where $\vec{\theta}^*$ denotes the parameters that minimize the cost function), thus showing an excellent convergence of the VQE algorithm. Note that similar ideal VQE simulations have been also performed using monomodal initial states (*i.e.* $|\Psi_{ini} = |4,0,0\rangle\rangle$ and $|\Psi_{ini}\rangle = |3,0,0,0\rangle$, not shown), and led to similar accuracy, demonstrating the ability of the BS-Kerr ansatz to efficiently map different initial states to the exact ground state of the attractive BH model (in all correlation regimes considered herein).

B. Ideal VQE v.s. realistic VQE with sampling noise: application to the BH dimer.

Let us now turn to the implementation of a more realistic execution of the VQE algorithm, as it could be done in a practical experiments.

1. Measure of the expectation value of the Hamiltonian by a photon counting approach

In practice, a realistic simulation of a VQE algorithm requires to measure the energy of a given trial state at the end of the quantum circuit. For this purpose, we propose a measurement protocol based on photon counting that can be realized using photon number resolving (PNR) detectors [79, 80], which are currently the most promising tools in quantum optics to efficiently measure a well-defined number of photons simultaneously. In the following, the notation $\langle \hat{O} \rangle_\Psi \equiv \langle \Psi | \hat{O} | \Psi \rangle$ is used and represents the quantum average of an operator $\hat{O}$ realized at

the end of the circuit when the photons are in the final state $|\Psi\rangle$.

Starting from the BH Hamiltonian $\hat{\mathcal{H}}$ defined in Eq. (1), measuring the energy of the final photonic state $|\Psi\rangle$ of the circuit requires measuring two different contributions,

$$\langle\hat{\mathcal{H}}_{\text{Hoppings}}\rangle = -J\sum_{\langle p,q\rangle}^{N_S}\langle(b_p^\dagger b_q + b_q^\dagger b_p)\rangle_\Psi, \qquad (17)$$

and

$$\langle\hat{\mathcal{H}}_{\text{Loc-Int}}\rangle = -\frac{U}{2}\sum_p^{N_S}\langle n_p(n_p - 1)\rangle_\Psi. \qquad (18)$$

The one-body (hopping) term in Eq. (17) can be measured by introducing additional 50/50 beam-splitter gates between each pair of modes before measuring, thus leading to

$$B_{p,q}(\pi/4,0)\left[b_p^\dagger b_q + b_q^\dagger b_p\right]B_{p,q}(\pi/4,0)^\dagger = n_q - n_p \quad (19)$$

such that

$$\langle b_p^\dagger b_q + b_q^\dagger b_p\rangle_\Psi = \langle n_q - n_p\rangle_{\tilde{\Psi}} \qquad (20)$$

where $|\tilde{\Psi}\rangle = B_{p,q}(\pi/4,0)|\Psi\rangle$. Thus, evaluating the hopping term between two modes with respect to the original trial state $|\Psi\rangle$ is equivalent to measuring the difference of average photon numbers in the two same modes after applying 50/50 beam-splitter.

Turning to the many-body interaction term in Eq. (18), note that it is directly related to the photon statistics of each individual mode at the end of the circuit:

$$\langle n_p(n_p - 1)\rangle_\Psi = \text{Var}(n_p)_\Psi + \langle n_p\rangle_\Psi^2 - \langle n_p\rangle_\Psi, \qquad (21)$$

where $\text{Var}(n_p) = \langle n_p^2\rangle_\Psi - \langle n_p\rangle_\Psi^2$ is the variance of the photon number in mode p at the end of the circuit. In other words, to estimate the contribution of the many-body interaction term to the total energy, we only need to evaluate (over many samples) the first two moments of the number operator for each mode p.

Although not studied in this work, note that extended versions of the BH model are sometimes considered (see for example Refs.[57, 81–83]), such as

$$\hat{\mathcal{H}}' = \hat{\mathcal{H}} + \sum_p \mu_p n_p + \sum_{p,q} V_{pq} n_p n_q, \qquad (22)$$

where μ_p is usually referred to as the "chemical potential", while the last term encodes the dipole-dipole interaction of two packets of bosons localized on different sites p and q. The expectation value of these two additional terms can also be estimated via photon counting. First, the expectation value of the one-body term containing the chemical potential

$$\langle\hat{\mathcal{H}}_{\text{Chem-Pot}}\rangle_\Psi = \sum_p \mu_p\langle n_p\rangle_\Psi \qquad (23)$$

is relatively simple to estimate as it only requires to do local photon-counting on each mode. The energy contribution of the dipole-dipole term

$$\langle\hat{\mathcal{H}}_{\text{dip-dip}}\rangle_\Psi = \sum_{p,q} V_{pq}\langle n_p n_q\rangle \qquad (24)$$

can be found by evaluating the covariance matrix of the photon number distribution in all the modes:

$$\langle n_p n_q\rangle = \text{Cov}(n_p, n_q) + \langle n_p\rangle\langle n_q\rangle. \qquad (25)$$

Note that setting $p = q$ in Eq. (25) gives back Eq. (21).

2. VQE with and without sampling noise

Focusing on the BH dimer, we now investigate how the sampling of the energy $E(\vec{\theta})$ can affect the quality of the VQE results. Compared to the ideal VQE simulations realized above, considering sampling noise leads to fluctuations in the energy $E(\vec{\theta})$ that makes the optimization harder in practice.

Fig. 16 shows the ground-state fidelity $\mathcal{F}$ obtained from VQE simulations with (right panel in blue) and without (left panel in green) sampling noise. In the latter case (with sampling noise), the energy is calculated using our photon-counting protocol described in Sec. V B 1. To mitigate the impact of noise in the classical optimization, we employed a "noise-proof" optimizer, namely CMA-ES [84]. The number of samples is fixed to 10^8 and photon-counting is only realized on the first mode of the circuit, as the conservation of the total number of bosons imposes $N_B = n_1 + n_2$ (i.e. measuring the number of photons n_1 in the first mode gives directly the number of photons n_2 in the second mode, assuming no photon loss).

Let us first focus on the ideal VQE simulation (left panel of Fig. 16). In analogy with the previous study in Sec. IV, the ground state is encoded with high fidelity whatever the initial state and correlation regime considered. In all of these cases, a sub-linear limit marks the separation between the regions of high and low fidelity-encoding (in average $N_L \approx 0.6 N_B$). The slope of this limit actually grows with the strength of Λ, thus indicating that "cat-like" states that arise for strong many-body interactions can be the more complex case to encode with a VQE using the BS-Kerr ansatz.

Turning to the noisy VQE simulation (right panel of Fig. 16) based on our photon-counting protocol, one can see that the resulting ground-state fidelity strongly depends on the nature of the initial state. Indeed, for $\Lambda \leq 5$, the results obtained with sampling noise are globally comparable to the ones from an ideal VQE. Interestingly, when the monomodal initial state is used, an even better fidelity is reached in this regime of weak correlation. However, for $\Lambda = 5$, the resulting fidelities
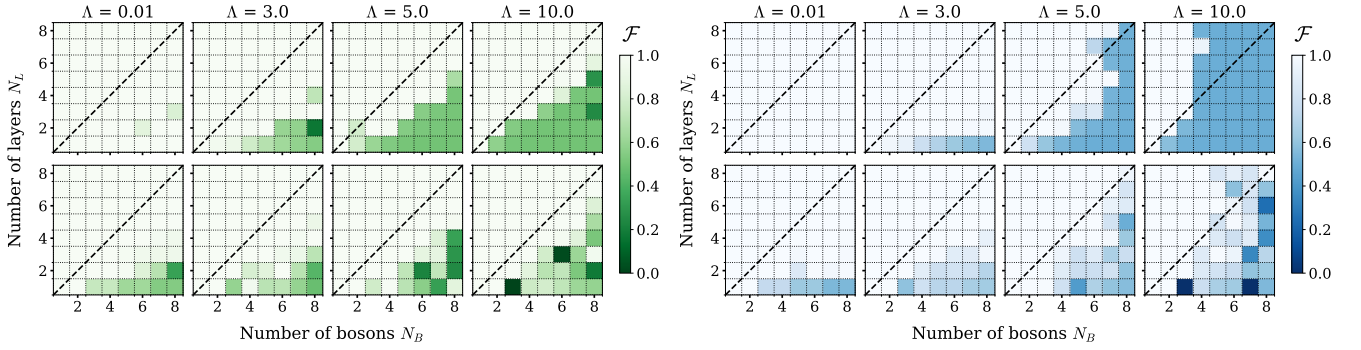
Figure 16. Ground-state fidelity $\mathcal{F}$ of the BH dimer obtained via VQE simulations using the BS-Kerr ansatz, as a function of the number of bosons N_B and the number of layers N_L, for different values of Λ. **Left panel:** noiseless VQE simulation using the BFGS optimizer with a maximum number of 2500 iterations. All parameters are initialized with a random amplitude in $[-1, +1]$. **Right panel:** VQE simulation with sampling noise using the noise-robust optimizer CMA-ES [84] with an initial step-size parameter of $\sigma_0 = 0.05$ and a maximum number of 20000 functions evaluations (each function evaluation stems from sampling of 10^8 samples of the quantum circuit). All parameters are initialized with a random amplitude in $[-0.1, +0.1]$. On each panel, upper and lower rows show results obtained by starting from a monomodal and a bimodal initial state, respectively.

deteriorate for both initial states, especially when the number of bosons increases. The deterioration is even more important when considering the strong interaction regime $\Lambda = 10$. In this case, a vertical limit separates the high- and low-fidelity regions at $N_B = 4$ when the monomodal initial state is used. Over this limits, the VQE trial state presents a fidelity of $\mathcal{F} \sim 50\%$ because it gets stuck in a single configuration of the cat-state during the optimization (*i.e.* the converged state was $|\Psi(\vec{\theta})\rangle \propto |N_B, 0\rangle$ instead of $|\Psi_0\rangle \propto |N_B, 0\rangle + |0, N_B\rangle$). Therefore, cat-like states seem difficult to realize by the BS-Kerr ansatz when sampling noise is considered. However, much better accuracy is reached when the bimodal initial state is used instead. Thus suggesting that starting from a configuration with photons spread in between the modes can improve the results of the VQE in the strongly correlated regime ($\Lambda \geq 5$ here). In summary, it seems from Fig. 16 that – within the BS-Kerr ansatz – a weakly-correlated state is more easily encoded when starting from a monomodal state rather than a bimodal one, and vice versa for a strongly-correlated state.

VI. CONCLUSIONS

In this work, we tackled the problem of encoding strongly correlated many-boson ground-state wavefunctions on a photonic quantum device. We designed two different quantum photonic-based ansatze and simulated a variational quantum algorithm (VQA) using the ground-state infidelity as a cost function. Both ansatze, the beam-splitter-Kerr (BS-Kerr) and the interferometer-Kerr, are based on layers of beam-splitter and Kerr gates, with additional rotation gates for the latter. We showed their ability to encode the ground state of the attractive BH model in all correlation regimes, for different number

of bosons and initial states. While the BS-Kerr ansatz has shown to be the most efficient in terms of total number of gates and parameters, it might not be optimal for conducting a true experiment on a real photonic quantum device, as it contains many Kerr gates that are difficult to implement in practice. In contrast, the interferometer-Kerr ansatz was designed to reduce the number of Kerr gates (or the number of layers required to achieve a given ground-state fidelity) at the expense of more rotation and beam-splitter gates and more parameters per layer, and is therefore more appropriate for realistic applications. Although taking the fidelity as a criteria is theoretically sound to test the encoding ability of our ansatze, in practice the cost function is the ground-state energy measured within the variational quantum eigensolver (VQE) algorithm. As a last investigation, we performed realistic VQE simulations using the BS-Kerr ansatz, with and without sampling noise, and proposed a photon-counting protocol to measure the ground-state energy of the BH Hamiltonian as it would be done in a real experiment. An even more realistic simulation should of course account for photon loss, on which error mitigation schemes can be applied [85]. This is left for future work.

Appendix A: Exact encoding of the BH ground state using only beam-splitters in the non-interacting limit

We demonstrate here that a single layer of the BS-Kerr ansatz, without the Kerr gates (so only beam-splitters) can exactly encode the ground state of the BH model for the three newtorks considered in our study (*i.e.* with $N_S = 2$, 3 and 4 sites) in the non-interacting limit $\Lambda \to 0$. Note that this demonstration works only for initial monomodal states such as $|N_B, 0\rangle$, $|N_B, 0, 0\rangle$ and $|N_B, 0, 0, 0\rangle$ for the dimer, three- and four-site BH model, respectively.

Let us start with the dimer, for which the exact ground state reads

$$|\Psi_0\rangle = \frac{1}{\sqrt{2N_B!}}[a_1^\dagger + a_2^\dagger]^{N_B} |0, 0\rangle. \tag{A1}$$

The action of a single layer of beam-splitter gates on an initial monomodal state results in

$$B_{1,2}(\theta, 0) |N_B, 0\rangle = \frac{1}{\sqrt{N_B!}}[\cos(\theta)a_0^\dagger + \sin(\theta)a_1^\dagger]^{N_B} |0, 0\rangle \tag{A2}$$

which provides an exact encoding of the ground state [Eq. (A1)] if we fix the beam-splitter transmittivity parameter to $\theta = \pi/4$. Turning to the three-site model, its exact ground state is given by

$$|\Psi_0\rangle = \frac{1}{\sqrt{3N_B!}}[a_1^\dagger + a_2^\dagger + a_3^\dagger]^{N_B} |0, 0, 0\rangle. \tag{A3}$$

applying the stair structure of the beam-splitters transform the initial monomodal state as follows,

$$\begin{aligned} B_{2,3}&(\theta', 0)B_{1,2}(\theta, 0) |N_B, 0, 0\rangle = \\ &\frac{1}{\sqrt{N_B!}}\Big[\cos(\theta)a_1^\dagger + \sin(\theta)\cos(\theta')a_2^\dagger \\ &+ \sin(\theta)\sin(\theta')a_3^\dagger \Big]^{N_B} |0, 0, 0\rangle, \end{aligned} \tag{A4}$$

thus realizing an exact encoding of the ground state [Eq. (A3)] when we fix the beam-splitter's parameters such that $\theta = \arccos(1/\sqrt{3})$ and $\theta' = \pi/4$. Finally, the exact ground state of the four-site model reads

$$|\Psi_0\rangle = \frac{1}{\sqrt{4N_B!}}[a_1^\dagger + a_2^\dagger + a_3^\dagger + a_4^\dagger]^{N_B} |0, 0, 0, 0\rangle. \tag{A5}$$

Similarly as for the BH dimer and three-site models, we apply a single layer of the BS-Kerr ansatz (without the Kerr) on the monomodal initial state, thus leading to

$$\begin{aligned} B_{3,4}&(\theta'', 0)B_{2,3}(\theta', 0)B_{1,2}(\theta, 0) |N_B, 0, 0, 0\rangle = \\ &\frac{1}{\sqrt{N_B!}}\Big[\cos(\theta)a_1^\dagger + \sin(\theta)\cos(\theta')a_2^\dagger \\ &+ \sin(\theta)\sin(\theta')\cos(\theta'')a_3^\dagger \\ &+ \sin(\theta)\sin(\theta')\sin(\theta'')a_4^\dagger) \Big]^{N_B} |0, 0, 0, 0\rangle. \end{aligned} \tag{A6}$$

Fixing the beam-splitter's parameters to $\theta = \pi/3$, $\theta' = \arccos(1/\sqrt{3})$ and $\theta'' = \pi/4$ generates an exact representation of the exact ground state in Eq.(A5).

[1] A. Peruzzo, J. McClean, P. Shadbolt, M.-H. Yung, X.-Q. Zhou, P. J. Love, A. Aspuru-Guzik, and J. L. O'brien, Nature Comm. **5**, 4213 (2014).

[2] P. J. O'Malley, R. Babbush, I. D. Kivlichan, J. Romero, J. R. McClean, R. Barends, J. Kelly, P. Roushan, A. Tranter, N. Ding, *et al.*, **6**, 031007 (2016).

[3] Y. Shen, X. Zhang, S. Zhang, J.-N. Zhang, M.-H. Yung, and K. Kim, Phys. Rev. A **95**, 020501 (2017).

[4] A. Kandala, A. Mezzacapo, K. Temme, M. Takita, M. Brink, J. M. Chow, and J. M. Gambetta, Nature **549**, 242 (2017).

[5] C. Hempel, C. Maier, J. Romero, J. McClean, T. Monz, H. Shen, P. Jurcevic, B. P. Lanyon, P. Love, R. Babbush, A. Aspuru-Guzik, R. Blatt, and C. F. Roos, **8**, 031022 (2018).

[6] J. I. Colless, V. V. Ramasesh, D. Dahlen, M. S. Blok, M. Kimchi-Schwartz, J. McClean, J. Carter, W. De Jong, and I. Siddiqi, **8**, 011021 (2018).

[7] G. Mazzola, P. J. Ollitrault, P. K. Barkoutsos, and I. Tavernelli, Phys. Rev. Lett. **123**, 130501 (2019).

[8] Y. Nam, J.-S. Chen, N. C. Pisenti, K. Wright, C. Delaney, D. Maslov, K. R. Brown, S. Allen, J. M. Amini, J. Apisdorf, *et al.*, npj Quantum Inf. **6**, 1 (2020).

[9] T. E. O'Brien, B. Senjean, R. Sagastizabal, X. Bonet-Monroig, A. Dutkiewicz, F. Buda, L. DiCarlo, and L. Visscher, npj Quantum Inf. **5**, 1 (2019).

[10] I. O. Sokolov, P. K. Barkoutsos, L. Moeller, P. Suchsland, G. Mazzola, and I. Tavernelli, Phys. Rev. Research **3**, 013125 (2021).

[11] F. Arute, K. Arya, R. Babbush, D. Bacon, J. C. Bardin, R. Barends, S. Boixo, M. Broughton, B. B. Buckley, D. A. Buell, B. Burkett, N. Bushnell, Y. Chen, Z. Chen, B. Chiaro, R. Collins, W. Courtney, S. Demura, A. Dunsworth, E. Farhi, A. Fowler, B. Foxen, C. Gidney, M. Giustina, R. Graff, S. Habegger, M. P. Harrigan, A. Ho, S. Hong, T. Huang, W. J. Huggins, L. Ioffe, S. V. Isakov, E. Jeffrey, Z. Jiang, C. Jones, D. Kafri, K. Kechedzhi, J. Kelly, S. Kim, P. V. Klimov, A. Korotkov, F. Kostritsa, D. Landhuis, P. Laptev, M. Lindmark, E. Lucero, O. Martin, J. M. Martinis, J. R. McClean, M. McEwen, A. Megrant, X. Mi, M. Mohseni, W. Mruczkiewicz, J. Mutus, O. Naaman, M. Neeley, C. Neill, H. Neven, M. Y. Niu, T. E. O'Brien, E. Ostby, A. Petukhov, H. Putterman, C. Quintana, P. Roushan, N. C. Rubin, D. Sank, K. J. Satzinger, V. Smelyanskiy, D. Strain, K. J. Sung, M. Szalay, T. Y. Takeshita, A. Vainsencher, T. White, N. Wiebe, Z. J. Yao, P. Yeh, and A. Zalcman, Science **369**, 1084 (2020).

[12] C. Cade, L. Mineh, A. Montanaro, and S. Stanisic, Physical Review B **102**, 235122 (2020).

[13] K. Fujii, K. Mitarai, W. Mizukami, and Y. O. Nakagawa, arXiv preprint arXiv:2007.10917 (2020).

[14] L. Xu, J. T. Lee, and J. Freericks, Modern Physics Letters B 34, 2040049 (2020).

[15] P. J. Ollitrault, A. Baiardi, M. Reiher, and I. Tavernelli, Chemical science 11, 6842 (2020).

[16] J. Romero and A. Aspuru-Guzik, Advanced Quantum Technologies 4, 2000003 (2021).

[17] H. R. Grimsley, S. E. Economou, E. Barnes, and N. J. Mayhall, arXiv preprint arXiv:1812.11173 (2018).

[18] H. L. Tang, V. Shkolnykov, G. Barron, H. Grimsley, N. Mayhall, E. Barnes, and S. Economou, Bulletin of the American Physical Society (2021).

[19] A. Montanaro and S. Stanisic, arXiv preprint arXiv:2006.01179 (2020).

[20] A. Masaki-Kato, S. Yunoki, and D. Hirashima, Physical Review B 100, 224515 (2019).

[21] W. Krauth, Physical review letters 77, 3695 (1996).

[22] A. Del Maestro and I. Affleck, Physical Review B 82, 060515 (2010).

[23] W. Purwanto and S. Zhang, Physical Review E 70, 056702 (2004).

[24] L. Pollet, Comptes Rendus Physique 14, 712 (2013).

[25] B. Bogner, C. De Daniloff, and H. Rieger, The European Physical Journal B 92, 1 (2019).

[26] M. Łącki, B. Damski, and J. Zakrzewski, Scientific reports 6, 1 (2016).

[27] K. Kawaki, Y. Kuno, and I. Ichinose, Physical Review B 95, 195101 (2017).

[28] N. Dogra, F. Brennecke, S. D. Huber, and T. Donner, Physical Review A 94, 023632 (2016).

[29] J.-P. Lv, Q.-H. Chen, and Y. Deng, Physical Review A 89, 013628 (2014).

[30] M. Rossi, M. Nava, L. Reatto, and D. Galli, The Journal of chemical physics 131, 154108 (2009).

[31] S. A. Wilkinson and M. J. Hartmann, Applied Physics Letters 116, 230501 (2020).

[32] P. Roushan, C. Neill, J. Tangpanitanon, V. M. Bastidas, A. Megrant, R. Barends, Y. Chen, Z. Chen, B. Chiaro, A. Dunsworth, A. Fowler, B. Foxen, M. Giustina, E. Jeffrey, J. Kelly, E. Lucero, J. Mutus, M. Neeley, C. Quintana, D. Sank, A. Vainsencher, J. Wenner, T. White, H. Neven, D. G. Angelakis, and J. Martinis, Science 358, 1175 (2017), https://science.sciencemag.org/content/358/6367/1175.full.pdf.

[33] S. Hacohen-Gourgy, V. V. Ramasesh, C. De Grandi, I. Siddiqi, and S. M. Girvin, Physical review letters 115, 240501 (2015).

[34] X.-H. Deng, C.-Y. Lai, and C.-C. Chien, Physical Review B 93, 054116 (2016).

[35] J. Huh, G. G. Guerreschi, B. Peropadre, J. R. McClean, and A. Aspuru-Guzik, Nature Photonics 9, 615 (2015).

[36] J. Huh and M.-H. Yung, Scientific reports 7, 1 (2017).

[37] C. Sparrow, E. Martín-López, N. Maraviglia, A. Neville, C. Harrold, J. Carolan, Y. N. Joglekar, T. Hashimoto, N. Matsuda, J. L. O'Brien, et al., Nature 557, 660 (2018).

[38] N. Quesada, J. Chem. Phys. 150, 164113 (2019).

[39] S. Jahangiri, J. M. Arrazola, N. Quesada, and A. Delgado, Phys. Chem. Chem. Phys. 22, 25528 (2020).

[40] T. Kalajdzievski, C. Weedbrook, and P. Rebentrost, Phys. Rev. A 97, 062311 (2018).

[41] H.-S. Zhong, H. Wang, Y.-H. Deng, M.-C. Chen, L.-C. Peng, Y.-H. Luo, J. Qin, D. Wu, X. Ding, Y. Hu, et al., Science 370, 1460 (2020).

[42] C. Weedbrook, S. Pirandola, R. García-Patrón, N. J. Cerf, T. C. Ralph, J. H. Shapiro, and S. Lloyd, Rev. Mod. Phys. 84, 621 (2012).

[43] T. R. Bromley, J. M. Arrazola, S. Jahangiri, J. Izaac, N. Quesada, A. D. Gran, M. Schuld, J. Swinarton, Z. Zabaneh, and N. Killoran, Quantum Sci. Technol. 5, 034010 (2020).

[44] O. Pfister, Journal of Physics B: Atomic, Molecular and Optical Physics 53, 012001 (2019).

[45] T. D. Kühner and H. Monien, Phys. Rev. B 58, R14741 (1998).

[46] T. D. Kühner, S. R. White, and H. Monien, Phys. Rev. B 61, 12474 (2000).

[47] M. W. Jack and M. Yamashita, Phys. Rev. A 71, 023610 (2005).

[48] N. Oelkers and J. Links, Physical Review B 75, 115119 (2007).

[49] B. Juliá-Díaz, D. Dagnino, M. Lewenstein, J. Martorell, and A. Polls, Physical Review A 81, 023615 (2010).

[50] M. Melé-Messeguer, B. Juliá-Díaz, and A. Polls, Journal of Low Temperature Physics 165, 180 (2011).

[51] O. Mansikkamäki, S. Laine, and M. Silveri, arXiv:2101.06032 (2021).

[52] M. Theis, G. Thalhammer, K. Winkler, M. Hellwig, G. Ruff, R. Grimm, and J. H. Denschlag, Physical Review Letters 93, 123001 (2004).

[53] K. Góral, L. Santos, and M. Lewenstein, Phys. Rev. Lett. 88, 170406 (2002).

[54] H. Büchler and G. Blatter, Phys. Rev. Lett. 91, 130404 (2003).

[55] I. Bloch, Nature Phys. 1, 23 (2005).

[56] I. Bloch, J. Dalibard, and W. Zwerger, Rev. Mod. Phys. 80, 885 (2008).

[57] S. Baier, M. J. Mark, D. Petter, K. Aikawa, L. Chomaz, Z. Cai, M. Baranov, P. Zoller, and F. Ferlaino, Science 352, 201 (2016).

[58] V. Pouthier, Phys. Rev. E 68, 021909 (2003).

[59] J. Edler, R. Pfister, V. Pouthier, C. Falvo, and P. Hamm, Phys. Rev. Lett. 93, 106405 (2004).

[60] D. Raventós, T. Graß, M. Lewenstein, and B. Juliá-Díaz, Journal of Physics B: Atomic, Molecular and Optical Physics 50, 113001 (2017).

[61] J. Zhang and R. Dong, European Journal of Physics 31, 591 (2010).

[62] B. Bauer and C. Nayak, Journal of Statistical Mechanics: Theory and Experiment 2013, P09005 (2013).

[63] M. Hopjan and F. Heidrich-Meisner, Physical Review A 101, 063617 (2020).

[64] O. Giraud, J. Martin, and B. Georgeot, Physical Review A 79, 032308 (2009).

[65] O. Giraud, J. Martin, and B. Georgeot, Physical Review A 76, 042333 (2007).

[66] A. Lukin, M. Rispoli, R. Schittko, M. E. Tai, A. M. Kaufman, S. Choi, V. Khemani, J. Léonard, and M. Greiner, Science 364, 256 (2019).

[67] R. Islam, R. Ma, P. M. Preiss, M. E. Tai, A. Lukin, M. Rispoli, and M. Greiner, Nature 528, 77 (2015).

[68] W. Beugeling, A. Andreanov, and M. Haque, Journal of Statistical Mechanics: Theory and Experiment 2015, P02002 (2015).

[69] M. Cerezo, A. Arrasmith, R. Babbush, S. C. Benjamin, S. Endo, K. Fujii, J. R. McClean, K. Mitarai, X. Yuan, L. Cincio, and P. J. Coles, arXiv:2012.09265 (2020).

[70] F. A. Evangelista, G. K.-L. Chan, and G. E. Scuseria,

The Journal of chemical physics **151**, 244112 (2019).

[71] I. O. Sokolov, P. K. Barkoutsos, P. J. Ollitrault, D. Greenberg, J. Rice, M. Pistoia, and I. Tavernelli, The Journal of chemical physics **152**, 124107 (2020).

[72] W. Mizukami, K. Mitarai, Y. O. Nakagawa, T. Yamamoto, T. Yan, and Y.-y. Ohnishi, Physical Review Research **2**, 033421 (2020).

[73] S. Yalouz, B. Senjean, J. Günther, F. Buda, T. E. O'Brien, and L. Visscher, Quantum Science and Technology **6**, 024004 (2021).

[74] R. W. Boyd, *Nonlinear optics* (Academic press, 2020).

[75] H. Azuma, J. Phys. D: Appl. Phys. **41**, 025102 (2007).

[76] W. R. Clements, P. C. Humphreys, B. J. Metcalf, W. S. Kolthammer, and I. A. Walmsley, Optica **3**, 1460 (2016).

[77] N. Killoran, J. Izaac, N. Quesada, V. Bergholm, M. Amy, and C. Weedbrook, Quantum **3**, 129 (2019).

[78] F. Gerber and R. Furrer, The R Journal **11**, 352 (2019).

[79] M. Jönsson and G. Björk, Physical Review A **99**, 043822 (2019).

[80] J. Provazník, L. Lachman, R. Filip, and P. Marek, Optics express **28**, 14839 (2020).

[81] W.-P. Chen, J. Singleton, L. Qin, A. Camón, L. Engelhardt, F. Luis, R. E. Winpenny, and Y.-Z. Zheng, Nature communications **9**, 1 (2018).

[82] D. Rossini and R. Fazio, New J. Phys. **14**, 065012 (2012).

[83] T. Ohgoe, T. Suzuki, and N. Kawashima, Physical Review B **86**, 054520 (2012).

[84] N. Hansen, arXiv preprint arXiv:1604.00772 (2016).

[85] D. Su, R. Israel, K. Sharma, H. Qi, I. Dhand, and K. Brádler, arXiv:2008.06670 (2020).